The Numerical Method of Characteristics for Electromagnetics

by

John H. Beggs *, David L. Marcum †, and Siew-Loong Chan
Mississippi State University
Department of Electrical and Computer Engineering &
MSU/NSF Engineering Research Center for Computational Field Simulation
Box 9571
Mississippi State, MS 39762

Abstract

The objective of this study is to explore the benefits of using the theory of characteristics to develop accurate and efficient numerical algorithms for Computational Electromagnetics. The present work adapts the numerical Method of Characteristics (MOC) from Computational Fluid Dynamics to the one-dimensional Maxwell curl equations in the time domain. The relevant theory of characteristics is developed and the inverse marching method is used to develop two numerical algorithms based on different interpolation schemes in the initial data surface. Stability and dispersion for these algorithms are discussed. Results are given for one-dimensional model problems involving free space pulse propagation, scattering from perfect conductors and reflection/transmission for lossy dielectric materials. The model problems are designed to provide quantitative insight into both accuracy and efficiency for different classes of realistic application problems. The Finite-Difference Time-Domain (FDTD) method is used as a convenient reference algorithm for comparison. It is demonstrated that these algorithms have accuracy comparable to FDTD, but do not require staggered grid storage, which simplifies impedance boundary conditions and implementation on nonuniform grids. The theory of characteristics demonstrates a very natural outer boundary condition without nonreflecting approximations or matched layers. A dispersion enhanced version of the MOC is also developed which has phase errors 50-5,000 times lower than FDTD. This approach appears promising for development of dispersion enhanced characteristic based schemes for two and three dimensional applications.

1 Introduction

Both small and large-scale transient electromagnetic phenomena are governed by the time dependent Maxwell equations. To properly develop numerical algorithms for approximate solutions to Maxwell's equations, it is important to separate the problem into three areas: the physics, the underlying mathematics and numerical algorithms. The physics, of course, are described by Maxwell's time dependent curl equations along with the constitutive relations for dielectric and magnetic media. Since Maxwell's equations are a system of hyperbolic partial differential equations (PDEs), the underlying mathematics is based upon the theory of characteristics. The theory of characteristics shows the solution at a given point in space and time has a finite domain of dependence and range of influence, and the boundary between these regions are characteristic curves. Once the underlying mathematics is defined and understood, a suitable numerical algorithm can be applied. Maxwell's time-dependent curl equations have typically been solved numerically by fixed grid finite difference or finite volume marching methods such as the Finite-Difference Time-Domain (FDTD) method [1]–[4] or Finite-Volume Time-Domain (FVTD) methods [5]–[19]. Many of these numerical methods have proceeded from a continuum version of Maxwell's equations directly to a discretized version by using various differencing schemes in time and space. This direct approach overlooks the theory of char-

*This work was sponsored in part by the NSF under Grant # EEC-8907070.

†DLM is with Mississippi State University, Department of Mechanical Engineering, P.O. Box ME, Mississippi State, MS 39762

acteristics, which provides a more natural path to a suitable numerical algorithm.

Numerical solutions of the Euler equations in Computational Fluid Dynamics (CFD) have illustrated the importance of treating a hyperbolic system of equations with the theory of characteristics. In a hyperbolic system, the solutions (e.g. waves) propagate in preferred directions called *characteristics*. A characteristic can be defined simply as a propagation path along which a physical disturbance is propagated [20]. The relevance to Maxwell's equations is intuitively obvious because electromagnetic waves have preferred directions of propagation and a finite propagation speed. For the one-dimensional wave equation,

$$\frac{\partial^2 \vec{E}}{\partial x^2} - c^2 \frac{\partial^2 \vec{E}}{\partial t^2} = 0 \qquad (1)$$

(where c is the speed of light) the solution involves propagating waves along the x coordinate with speeds of $\pm c$. In general, the characteristic curves are $(n-1)$-dimensional hyper-surfaces in n-dimensional hyper-space (with n as the number of independent variables) [21]. For the wave equation in (1), the characteristics in the two-dimensional solution domain are straight lines.

Characteristic based methods offer substantial benefits over traditional fixed grid finite difference or finite volume schemes. First, characteristic based methods treat the outer boundary condition naturally without nonreflecting approximations or matched layers. The interior point algorithm predicts the outgoing characteristic variables, and the algorithm only requires information about the incoming characteristic variables at the domain boundaries. Through knowledge of the wave propagation angle, the local coordinates can be rotated to align with the characteristics, at which point the boundary condition becomes almost exact. Therefore, no extraneous boundary condition is required to introduce additional information into the solution. Second, characteristic based methods are typically more accurate for the same order of finite difference equation. This is because a characteristic based method closely follows the direction of information propagation in the physical space, which provides increased accuracy. Finally, characteristic based algorithms for CEM can easily be parametrically combined to reduce phase errors without using higher order difference schemes. Ultimately, the theory of characteristics should provide the most natural path toward a numerical scheme for CEM.

The objective of this paper is to elucidate the benefits of using a characteristic based formulation to numerically solve Maxwell's equations by development, implementation and testing of two method of characteristics algorithms on one dimensional propagation and scattering problems. These model problems show relevance to the complex multidimensional applications and the results are compared with analytical solutions or FDTD simulations. An enhanced version of the numerical MOC is also presented that has phase errors 50-5,000 times lower than FDTD.

2 One-dimensional MOC Algorithm

The numerical Method of Characteristics (MOC) has been used successfully for gas dynamics problems in Computational Fluid Dynamics (CFD) [22]–[27] and is very suitable for electromagnetics problems. In fact, CFD researchers Shankar *et al.* [28]–[33] and Shang *et al.* [34]–[43] were the first to recognize the importance of using a characteristic based algorithm for Maxwell's equations. Their work concentrated on development of both explicit and implicit characteristic based finite volume CFD methods for CEM. This work intends to provide an electrical engineering perspective on the theory of characteristics; and at the same time, develops different finite difference characteristic based algorithms.

The method of characteristics is essentially a coordinate transformation in which the computational coordinates (the characteristic surfaces) are also the paths of propagation of information in the physical space. The governing PDEs are replaced by an equivalent set of characteristic equations and the applicable compatibility equations. The characteristic equations are first integrated to construct the characteristic coordinate system. Next, the compatibility equations are integrated along the characteristic curves to give the distribution of the dependent variable on the characteristic curves. Finally, the inverse-marching method is then used to determine the required elements in the initial data surface [21]. The MOC model provides a direct match between the numerical and physical propagation paths. In contrast, fixed-grid finite-difference methods (such as FDTD) propagate information only along coordinate axes, but they do propagate

energy along the physical propagation paths. The MOC also separately treats waves propagating in opposite directions, and uses differencing schemes based upon those directions.

One set of Maxwell's equations for linear and homogeneous media in the one dimensional case (taking $\partial/\partial y = \partial/\partial z = 0$) are

$$\frac{\partial E_y}{\partial t} + \frac{1}{\epsilon}\frac{\partial H_z}{\partial x} = -\frac{\sigma}{\epsilon}E_y \quad (2)$$

$$\frac{\partial H_z}{\partial t} + \frac{1}{\mu}\frac{\partial E_y}{\partial x} = 0 \quad (3)$$

These equations can be rearranged in a more convenient form given by

$$\frac{\partial E_y}{\partial t} + Z_i c\frac{\partial H_z}{\partial x} = -\frac{\sigma}{\epsilon}E_y \quad (4)$$

$$\frac{\partial H_z}{\partial t} + \frac{c}{Z_i}\frac{\partial E_y}{\partial x} = 0 \quad (5)$$

where $c = 1/\sqrt{\mu\epsilon}$ is the speed of light in the medium and $Z_i = \sqrt{\mu/\epsilon}$ is the intrinsic wave impedance of the medium. Applying the chain rule to the continuous functions $E_y(x,t)$ and $H_z(x,t)$ gives

$$dE_y = \frac{\partial E_y}{\partial t}dt + \frac{\partial E_y}{\partial x}dx \quad (6)$$

$$dH_z = \frac{\partial H_z}{\partial t}dt + \frac{\partial H_z}{\partial x}dx \quad (7)$$

Putting equations (4)–(7) into matrix form gives

$$\begin{bmatrix} 1 & 0 & 0 & Z_i c \\ 0 & c/Z_i & 1 & 0 \\ dt & dx & 0 & 0 \\ 0 & 0 & dt & dx \end{bmatrix} \begin{bmatrix} \frac{\partial E_y}{\partial t} \\ \frac{\partial E_y}{\partial x} \\ \frac{\partial H_z}{\partial t} \\ \frac{\partial H_z}{\partial x} \end{bmatrix} = \begin{bmatrix} -\frac{\sigma}{\epsilon}E_y \\ 0 \\ dE_y \\ dH_z \end{bmatrix} \quad (8)$$

Setting the determinant of the coefficient matrix equal to 0 gives the characteristic equation of the system as

$$dx^2 - c^2dt^2 = 0 \quad (9)$$

Solving this equation yields the solutions

$$\frac{dx}{dt} = \pm c \quad (10)$$

These are the characteristic equations of the system. They provide two distinct real roots of the characteristic equation, which is typical of a system of hyperbolic equations. Equation (10) also shows that waves propagate in the $\pm x$ directions with a finite physical speed of c.

For the continuous function $E_y(x,t)$, the total differential is defined by

$$dE_y = \frac{\partial E_y}{\partial t}dt + \frac{\partial E_y}{\partial x}dx = \left(\frac{\partial E_y}{\partial t} + \frac{dx}{dt}\frac{\partial E_y}{\partial x}\right)dt \quad (11)$$

Using (10), this can be rewritten as

$$\frac{dE_y}{dt} = \left(\frac{\partial E_y}{\partial t} \pm c\frac{\partial E_y}{\partial x}\right) \quad (12)$$

The total derivative along the characteristic is then defined by

$$\frac{D_\pm(\cdot)}{Dt} = \frac{\partial(\cdot)}{\partial t} \pm c\frac{\partial(\cdot)}{\partial x} \quad (13)$$

A similar relationship can be developed for H_z to give

$$\frac{dH_z}{dt} = \left(\frac{\partial H_z}{\partial t} \pm c\frac{\partial H_z}{\partial x}\right) \quad (14)$$

Using (13) and taking a linear combination of equations (12) and (14) gives

$$\frac{D_+(E_y)}{Dt} + Z_i\frac{D_+(H_z)}{Dt} = -\frac{\sigma}{\epsilon}E_y \quad (15)$$

for the right-going characteristic and

$$\frac{D_-(E_y)}{Dt} - Z_i\frac{D_-(H_z)}{Dt} = -\frac{\sigma}{\epsilon}E_y \quad (16)$$

for the left-going characteristic. These characteristic curves are straight lines in the two-dimensional solution space (x,t) and are shown in Figure 1. Equations (15) and (16) are the compatibility equations for the system. To integrate these equations along the characteristic curves, they are treated as

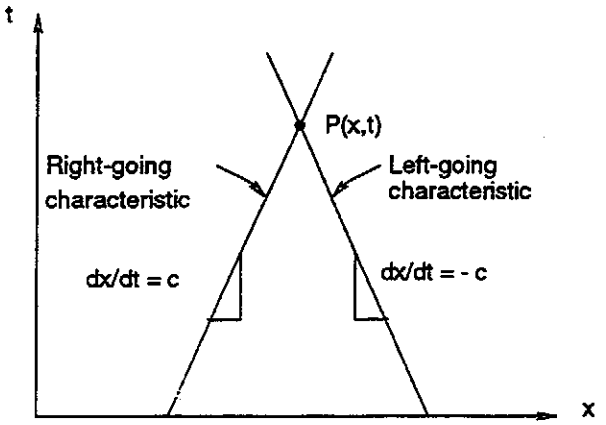

Figure 1: Two dimensional solution domain $D(x,t)$ showing right and left-going characteristics.

a system of ordinary differential equations (ODEs). Thus, equations (15) and (16) now become

$$dE_y + Z_i dH_z = -\frac{\sigma}{\epsilon} E_y dt \quad \text{along } D_+ \tag{17}$$

$$dE_y - Z_i dH_z = -\frac{\sigma}{\epsilon} E_y dt \quad \text{along } D_- \tag{18}$$

The characteristic equations from (10) can be rewritten in ODE format as

$$dx = cdt \quad \text{along } D_+ \tag{19}$$

$$dx = -cdt \quad \text{along } D_- \tag{20}$$

A prespecified, two-dimensional, space-time grid is now defined in the solution domain $D(x,t)$ with coordinates $x = i\Delta x$ and $t = n\Delta t$ as shown in Figure 2. The inverse marching method is employed to numerically integrate equations (17)–(20) to determine the solution at point P (see Figure 2). From the point P at coordinates $(i, n+1)$, the characteristics are projected rear-ward onto the initial data surface at time level n. The x-intercepts may or may not intersect the initial data surface at prespecified grid points; therefore, interpolation in the initial data surface is, in general, required. Equations (19) and (20) are first integrated to give

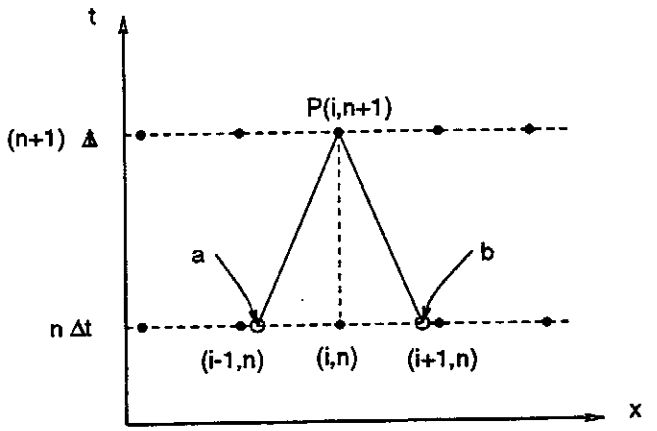

Figure 2: Two dimensional space-time grid showing solution point P with characteristics projected rearward onto initial data surface at points a and b.

$$x_a = x_i - c\Delta t \tag{21}$$

$$x_b = x_i + c\Delta t \tag{22}$$

Integrating the compatibility equations in (17) and (18) gives

$$\left(E_y^P - E_y^a\right) + Z_i\left(H_z^P - H_z^a\right) = -\frac{\sigma}{\epsilon} E_y^P \Delta t \tag{23}$$

$$\left(E_y^P - E_y^b\right) - Z_i\left(H_z^P - H_z^b\right) = -\frac{\sigma}{\epsilon} E_y^P \Delta t \tag{24}$$

These equations are solved simultaneously for E_y^P to give

$$E_y^P = A_1\left(E_y^a + E_y^b\right) - A_2\left(H_z^b - H_z^a\right) \tag{25}$$

where

$$A_1 \equiv \frac{1}{2\left(1 + \sigma\Delta t/\epsilon\right)}, \quad A_2 \equiv \frac{Z_i}{2\left(1 + \sigma\Delta t/\epsilon\right)} \tag{26}$$

Note that for a perfect electrical conductor as $\sigma \to \infty$, $A_1 = A_2 = 0.0$, which properly enforces the perfect conductor boundary condition in (25). The solution of (23) and (24) for H_z^P is

$$H_z^P = \frac{1}{2}\left(H_z^a + H_z^b\right) - A_3\left(E_y^b - E_y^a\right) \tag{27}$$

where $A_3 \equiv 1/(2Z_i)$. At this point, the solution is complete except for obtaining the values of E_y and H_z at points a and b. Two algorithms are now presented based upon different interpolation schemes in the initial data surface to obtain these field values at points a and b.

2.1 MOC Algorithm 1

For the first MOC algorithm, quadratic interpolation using a second-order Lagrange polynomial is performed in the initial data surface using grid points $(i-2,n)$, $(i-1,n)$ and (i,n) for the field component at point a. For the field at point b, grid points (i,n), $(i+1,n)$ and $(i+2,n)$ are used. This interpolation scheme was chosen to provide an upwind, second-order interpolation formula which has equivalent order of accuracy as the FDTD method. With this interpolation scheme, the electric field intensities at points a and b are given by

$$E_y^a = E_y^n(i) + \frac{\nu^2}{2}\left(E_y^n(i) - 2E_y^n(i-1) + E_y^n(i-2)\right) - \frac{\nu}{2}\left(3E_y^n(i) - 4E_y^n(i-1) + E_y^n(i-2)\right) \tag{28}$$

$$E_y^b = E_y^n(i) + \frac{\nu^2}{2}\left(E_y^n(i) - 2E_y^n(i+1) + E_y^n(i+2)\right) - \frac{\nu}{2}\left(3E_y^n(i) - 4E_y^n(i+1) + E_y^n(i+2)\right) \tag{29}$$

with $\nu \equiv (c\Delta t)/\Delta x$. Similar equations are derived for the magnetic field intensities, H_z^a and H_z^b. These equations are then used in (25) and (27) to complete the algorithm implementation. This algorithm has conditional stability of $\nu \leq 1$ and has accuracy $O\left(\Delta t^2, \Delta x^2\right)$.

For nonuniform grids, quadratic interpolation gives the following formulas for E_y^a and E_y^b:

$$E_y^a = \frac{c\Delta t\,(c\Delta t - \Delta x_{i-1})}{\Delta x_{i-2}\,(\Delta x_{i-2} + \Delta x_{i-1})} E_y^n(i-2) + \frac{c\Delta t\,(\Delta x_{i-2} + \Delta x_{i-1} - c\Delta t)}{\Delta x_{i-2}\Delta x_{i-1}} E_y^n(i-1) + \frac{(\Delta x_{i-2} + \Delta x_{i-1} - c\Delta t)\,(\Delta x_{i-1} - c\Delta t)}{(\Delta x_{i-2} + \Delta x_{i-1})\,\Delta x_{i-1}} E_y^n(i) \quad (30)$$

$$E_y^b = \frac{(c\Delta t - \Delta x_i)\,(c\Delta t - (\Delta x_i + \Delta x_{i+1}))}{\Delta x_i\,(\Delta x_i + \Delta x_{i+1})} E_y^n(i) - \frac{c\Delta t\,(c\Delta t - (\Delta x_i + \Delta x_{i+1}))}{\Delta x_i \Delta x_{i+1}} E_y^n(i+1) + \frac{c\Delta t\,(c\Delta t - \Delta x_i)}{(\Delta x_i + \Delta x_{i+1})\,\Delta x_{i+1}} E_y^n(i+2) \quad (31)$$

with the definition $\Delta x_i \equiv x_{i+1} - x_i$.

2.2 MOC Algorithm 2

For the second MOC algorithm, quadratic interpolation is also performed using grid points $(i-1, n)$, (i, n) and $(i+1, n)$ for the field components at points a and b. This interpolation scheme was chosen again to provide second order accuracy, but it adds one downwind point, which provides a lagging phase error. This is in contrast to the upwind interpolation scheme in the previous section, which has a leading phase error. These two schemes are combined together in Section 5. For the electric field intensity, this interpolation scheme gives

$$E_y^a = E_y^n(i) - \frac{\nu}{2}\left(E_y^n(i+1) - E_y^n(i-1)\right) + \frac{\nu^2}{2}\left(E_y^n(i+1) - 2E_y^n(i) + E_y^n(i-1)\right) \quad (32)$$

$$E_y^b = E_y^n(i) + \frac{\nu}{2}\left(E_y^n(i+1) - E_y^n(i-1)\right) + \frac{\nu^2}{2}\left(E_y^n(i+1) - 2E_y^n(i) + E_y^n(i-1)\right) \quad (33)$$

with similar relationships for the magnetic field intensity. Equations (25) and (27) now become

$$E_y^{n+1}(i) = 2A_1 E_y^n(i) - A_2\nu\left(H_z^n(i+1) - H_z^n(i-1)\right) + \nu^2 A_1\left(E_y^n(i+1) - 2E_y^n(i) + E_y^n(i-1)\right) \quad (34)$$

$$H_z^{n+1}(i) = H_z^n(i) - \nu A_3\left(E_y^n(i+1) - E_y^n(i-1)\right) + \frac{\nu^2}{2}\left(H_z^n(i+1) - 2H_z^n(i) + H_z^n(i-1)\right) \quad (35)$$

This algorithm is equivalent to the Lax-Wendroff one-step method with conditional stability $\nu \leq 1$ and with accuracy $O(\Delta t^2, \Delta x^2)$.

For nonuniform grids, quadratic interpolation gives the following formulas for E_y^a and E_y^b:

$$E_y^a = \frac{c\Delta t\,(c\Delta t + \Delta x_i)}{\Delta x_{i-1}\,(\Delta x_{i-1} + \Delta x_i)} E_y^n(i-1) - \frac{(c\Delta t - \Delta x_{i-1})\,(c\Delta t + \Delta x_i)}{\Delta x_i \Delta x_{i-1}} E_y^n(i) + \frac{c\Delta t\,(c\Delta t - \Delta x_{i-1})}{\Delta x_i\,(\Delta x_{i-1} + \Delta x_i)} E_y^n(i+1) \quad (36)$$

$$E_y^b = \frac{c\Delta t\,(c\Delta t - \Delta x_i)}{\Delta x_{i-1}\,(\Delta x_{i-1} + \Delta x_i)} E_y^n(i-1) - \frac{(c\Delta t + \Delta x_{i-1})\,(c\Delta t - \Delta x_i)}{\Delta x_{i-1}\Delta x_i} E_y^n(i) + \frac{c\Delta t\,(c\Delta t + \Delta x_{i-1})}{\Delta x_i\,(\Delta x_{i-1} + \Delta x_i)} E_y^n(i+1) \quad (37)$$

2.3 Perfect Conductor Boundary Condition

For perfect conductor boundaries, the characteristic update equations must be modified accordingly. Referring to Figure 2, if a perfect electrical conductor (PEC) half space begins at grid point i and extends to the right boundary of the problem space, then the following conditions apply

$$E_y^b = H_z^b = E_y^P = E_y^{n+1}(i) = 0.0 \quad (38)$$

With these conditions, the equation for H_z at point P (see Figure 2) in (27) now becomes

$$H_z^P = \frac{1}{2}H_z^a + A_3 E_y^a \quad (39)$$

A suitable and accurate update equation for a perfectly conducting boundary can be derived and is given by

$$H_z^P = H_z^{n+1}(i) = \nu H_z^n(i-1) + (1-\nu)\,H_z^n(i) + \nu A_3 E_y^n(i-1) \quad (40)$$

This equation, along with the conditions in (38), form the necessary implementation for a perfectly conducting boundary. A similar equation can be developed for a left-sided PEC half space starting at cell i and continuing to the beginning of the computational domain.

2.4 Boundary Conditions

Since the MOC algorithms use the theory of characteristics, no extraneous boundary condition

such as the Liao absorbing boundary condition [44] or the PML [45] is required. This is a significant advantage over fixed grid finite difference or finite volume methods. For example, the FDTD method uses a spatial central difference operator, which for a wave propagating from left to right, eventually requires a grid point *outside* the domain. This requirement introduces an additional equation (i.e. boundary condition) to solve the system and introduces information into the solution that is not required by Maxwell's equations. Using an upwind characteristic based approach, the interior point algorithm calculates the left-going characteristic at the left boundary (i.e. at $i = 0$) and the right-going characteristic at the right boundary (i.e. at $i = imax$). Therefore, the only additional information required is for waves *entering* the domain. Waves exiting the domain are handled naturally by the interior point algorithm. Therefore, the characteristic boundary conditions are as follows: at grid point $i = 0$, equation (29) is used to calculate $E_y^b(0)$. Then, equation (25) is used, along with a specification of the incoming, right-going field, $E_y^a(0)$. Therefore, the interior point algorithm of (29) calculates the outgoing, left-traveling field at the $i = 0$ boundary, and the incoming, right-going field is specified as a boundary condition. A similar analysis applies at the right grid boundary. At grid point $i = imax$, equation (28) is used to calculate $E_y^a(imax)$. Then, equation (25) is used, along with a specification of the incoming, left-going field, $E_y^b(imax)$. Therefore, the interior point algorithm of (28) calculates the outgoing, right-traveling field, and the incoming, left-going field is specified as a boundary condition. Thus, the only additional information introduced at the boundary is nothing more than what is required by the physical system. A similar analysis holds for characteristic boundary conditions for two and three-dimensional situations. For grid points $i = 1$ and $i = imax - 1$, a first-order accurate interpolation scheme is employed for the right-going (equation (28)) characteristic and left-going (equation (29)) characteristic, respectively.

The boundary conditions outlined in this section are exact for one-dimensional wave propagation because the characteristic wave motion is aligned with a Cartesian axis. For two and three-dimensional simulations, characteristic based methods can be split into a set of one-dimensional operators corresponding to the eigenvalues of the system. In this case, these one-dimensional operators provide an exact boundary condition if the wave motion is aligned with a Cartesian axis. In the general case, the wave propagation angle can be estimated using the Poynting vector $\left(\vec{E} \times \vec{H}^*\right)$, and then a coordinate transformation can be applied to align the wave propagation angle with a Cartesian grid axis. However, details of this coordinate transformation have not yet been outlined, and this will be the subject of a future article.

3 Fourier Analysis

One of the main measures in characterizing an EM algorithm is its dispersion properties. Substituting trial solutions of the form $E_y^n(i) = E_0 e^{j(\omega n\Delta t - ki\Delta x)}$ and $H_z^n(i) = E_y^n(i)/\eta_0$ into the update equations for each MOC method, the following dispersion relationships are derived:

$$f_1(k) = e^{j\omega\Delta t} + \frac{\nu}{2}(1-\nu)e^{j2k\Delta x} - \nu(2-\nu)e^{jk\Delta x} - 1 - \frac{\nu^2}{2} + \frac{3}{2}\nu \quad \text{MOC1} \tag{41}$$

$$f_2(k) = e^{j\omega\Delta t} - (1-\nu^2) - \nu^2\cos k\Delta x - j\nu\sin k\Delta x \quad \text{MOC2} \tag{42}$$

These equations are numerically solved for the wavenumber k using a Newton iteration procedure as

$$k^*_{m+1} = k^*_m - \frac{f'(k^*_m)}{f(k^*_m)} \tag{43}$$

where m denotes the iteration number and k^* denotes the numerical wavenumber. The phase error is computed as a ratio of the numerical wavenumber, k^*, to the exact wavenumber, k. Figure 3 shows the dispersion of the MOC algorithms as compared to FDTD versus grid resolution using $\nu = 3/4$. Note

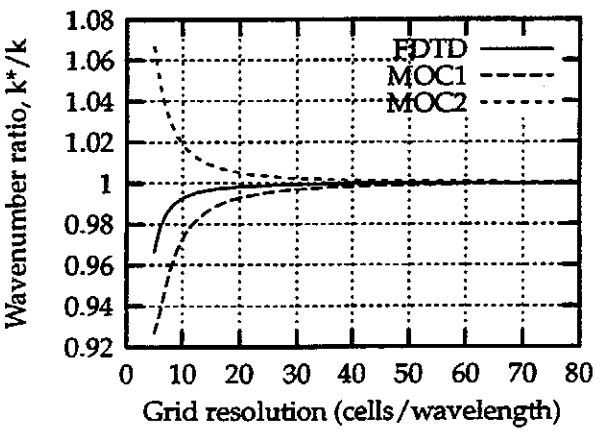

Figure 3: Numerical dispersion versus grid resolution for FDTD and the Method of Characteristics schemes with $\nu = 3/4$.

that algorithm MOC1 has leading phase error and MOC2 has a lagging phase error similar to the FDTD method. From the graph, it appears that these MOC methods are less accurate than FDTD, but the relative accuracy of the characteristic based schemes are about the same.

4 Results

These MOC algorithms were employed to simulate pulse propagation in free space and also to simulate reflection and transmission for perfectly conducting and lossy dielectric materials. Results for these problems were compared with FDTD simulations. For pulse propagation, the problem space size was 2000 cells with periodic boundary conditions, a uniform grid of 1 cm cell size, and a time step of 25 ps. The periodic boundary conditions enforced were that $E_y(i = 2000) = E_y(i = 0)$, which makes the one-dimensional problem space a closed ring. A Gaussian pulse with a full-width half-maximum (FWHM) pulse width of 1.8 ns was used and it contained significant frequency content up to 1 GHz. The Courant number was $\nu = 0.75$, and the pulse was allowed to propagate for a distance of 100λ at 1 GHz, which corresponds to approximately 30 meters. Figure 4 shows the error in the electric field results for the MOC algorithms and FDTD obtained by subtracting the numerical results from the exact solution after 4000 time steps. The

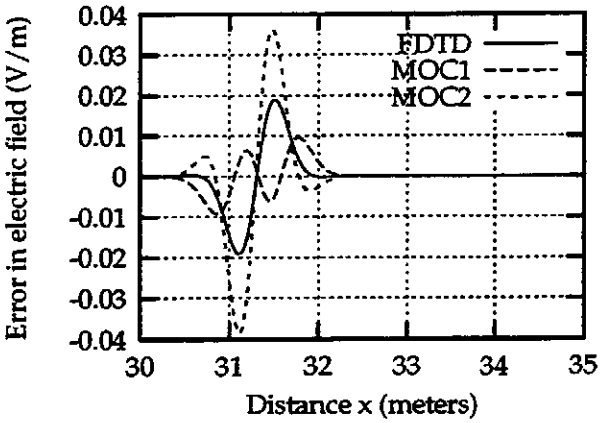

Figure 4: Error in electric field for free space pulse propagation using FDTD and the MOC algorithms with periodic boundary conditions.

MOC1 algorithm has approximately 1/2 the error as FDTD for this problem, which can be attributed to the windward interpolation scheme in the initial data surface. The MOC2 algorithm had less accurate results than FDTD due to the centered interpolation scheme. Even though the MOC algorithms have more phase error than FDTD, they still provide very accurate results, which is an inherent benefit of the characteristic formulation. It is useful to note that combining (21) and (22) with the definition of the Courant number $\nu = (c\Delta t)/\Delta x$ yields,

$$\nu = (x_i - x_a)/\Delta x = (x_b - x_i)/\Delta x \qquad (44)$$

If the characteristic intersects the initial data surface at the prescribed grid points, then $\nu = 1$; and, for a uniform grid, the MOC algorithms gave identical results as FDTD, with no dissipation or dispersion. The same propagation problem was simulated using a *nonuniform* grid with a mesh stretch ratio, $M_s \equiv \Delta x_{max}/\Delta x_{min}$ of 2, which was periodic every 10 cells. The pulse propagated the same distance of 30 meters, with $\nu = 1$. The Courant number, ν, for a nonuniform grid, was defined by $c\Delta t/\Delta x_{min}$, where Δx_{min} is the smallest cell size in the nonuniform grid. Figure 5 shows the error in electric field versus distance x obtained by subtracting the numerical results from the analytical solution. Note how the FDTD results show error

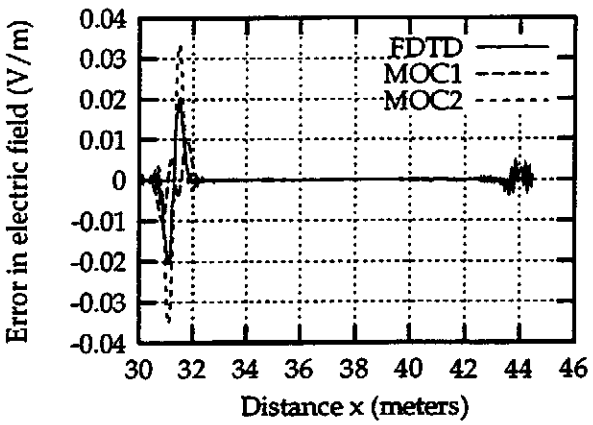

Figure 5: Error in electric field for free space pulse propagation using FDTD and the MOC algorithms with periodic boundary conditions on a nonuniform grid with $\nu = 1$ and a mesh stretch ratio of 2:1 over 10 cells.

away from the area of the main pulse. The MOC1 results are more accurate than FDTD, which again is a benefit of the windward interpolation scheme. The MOC2 results exhibit similar accuracy behavior as the uniform grid case.

For the next problem, a perfectly conducting half-space was inserted for $7.5 \leq x \leq 20$ m, with the problem space and incident pulse having the same parameters as before. The total electric field was

again sampled at $x = 4$ m. Using the PEC boundary condition in (40), the MOC algorithms produce the results shown in Figure 6 with a Courant number of $\nu = 0.75$. Note the agreement is excellent for

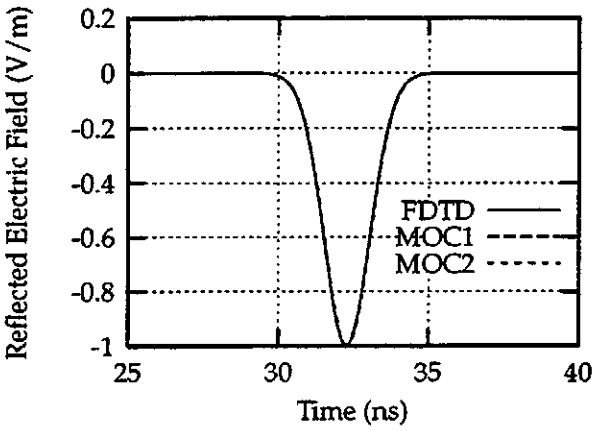

Figure 6: Reflected electric field versus time at a perfectly conducting half-space using FDTD and the MOC algorithms.

both reflected pulses. Even better agreement was observed for a Courant number of $\nu = 1$.

To verify treatment of lossy dielectric materials with the MOC algorithms, a lossy dielectric layer was inserted for $5 \leq x \leq 6$ m with material parameters $\epsilon_r = 4$ and $\sigma = 0.002$. Again, the incident pulse was a Gaussian with FWHM pulse width of 1.8 ns and the Courant number was again $\nu = 3/4$. Figure 7 shows the total field at $x = 4$ m, Figure 8 shows the transmitted field inside the sheet at $x = 5.5$ m and Figure 9 shows the transmitted field on the right side of the sheet at $x = 7.5$ m.

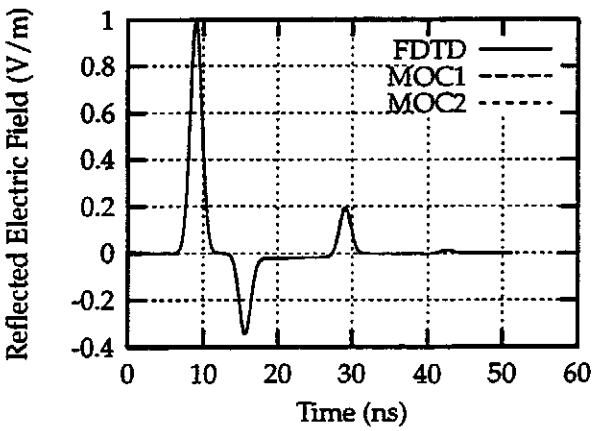

Figure 7: Reflected electric field versus time at $x = 4$ m for scattering from a lossy dielectric layer.

Note the results for the MOC algorithms are

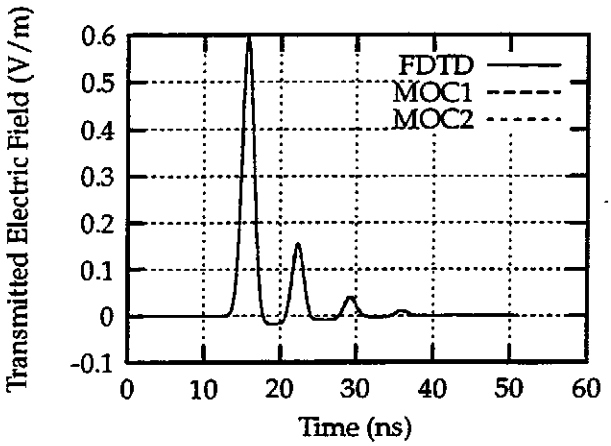

Figure 8: Transmitted electric field versus time at $x = 5.5$ m for scattering from a lossy dielectric layer.

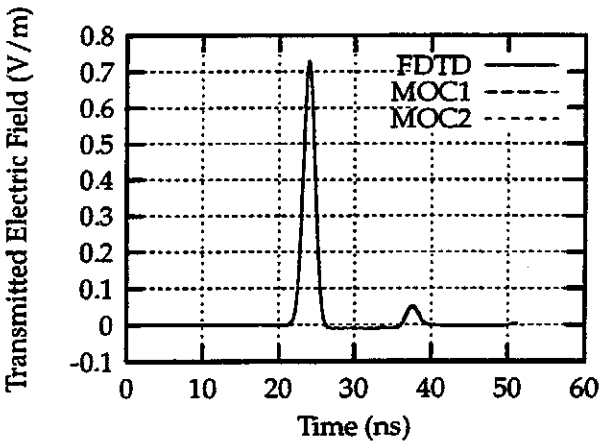

Figure 9: Transmitted electric field versus time at $x = 7.5$ m for scattering from a lossy dielectric layer.

indistinguishable from the FDTD results in all three figures. This shows that the MOC algorithms have accuracy equivalent to that of the FDTD method, but using a characteristic based scheme which propagates information directly along the physical propagation paths.

These one-dimensional model problem results have demonstrated that the numerical MOC is promising for extension and application to realistic three-dimensional problems involving PEC and lossy dielectric materials. The MOC algorithms also gave excellent results when tested on nonuniform grids, which further demonstrates these results have relevance to complex multi-dimensional applications.

5 Dispersion Enhanced MOC Scheme

The phase error of the MOC scheme can be significantly improved by combining the leading and lagging phase errors of both MOC schemes parametrically for a dispersion error lower than any almost any other higher order finite difference scheme currently available for solving Maxwell's equations. This technique was first used by Fromm [46] for CFD in which he performed a simple average of forward and backward time steps to minimize dispersion for explicit convective difference schemes. The idea of dispersion enhancement has appeared periodically in CEM [3], [47], [48], but not in the context of cancellation of leading and lagging phase errors. Lele [49] and Gaitonde and Shang [50] also performed dispersion enhancement for compact difference schemes. Fromm reduced the dispersion error by a factor of 10 over a standard second-order scheme, and the error was even lower than a standard fourth-order method. The present work generalizes Fromm's approach by performing a weighted average using a parameter, α ($0 \leq \alpha \leq 1$), which interpolates between the two wavenumber equations (41) and (42) to give a combined dispersion relationship of

$$f_0(k) = (1-\alpha) f_1(k) + \alpha f_2(k) \qquad (45)$$

This equation is numerically solved for the enhanced wavenumber, k_o^*, using the Newton iteration procedure given in (43). The enhanced scheme uses a 5-point stencil at grid points $i-2$, $i-1$, i, $i+1$ and $i+2$. This same technique can also be used with different interpolation schemes in the initial data surface to provide a dispersion enhanced scheme using only a 3-point stencil at points $i-1$, i and $i+1$. Equation (45) was optimized for a specific wavenumber and Courant number by performing a numerical search of α to minimize the mean square error in numerical wavenumber over grid resolutions ranging from 20 to 80 cells per wavelength. The optimum value of α was found to be $\alpha = 0.419$ for $\nu = 3/4$ and $\alpha = 0.5$ for $\nu = 1/2$. Using these optimum α's, Figures 10 and 11 show the percent error in wavenumber (i.e. numerical dispersion) of the enhanced scheme and FDTD versus grid resolution for $\nu = 3/4$ and $\nu = 1/2$, respectively.

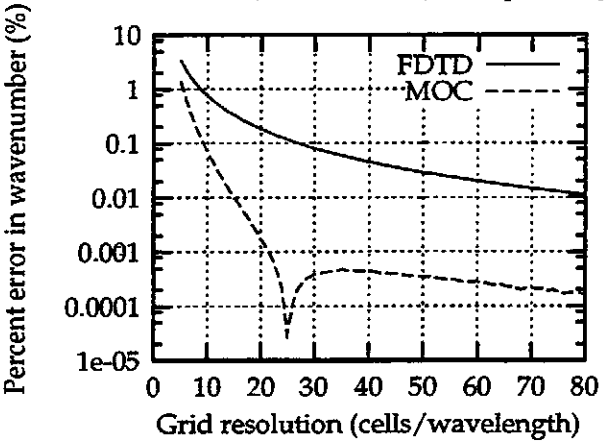

Figure 10: Percent error in wavenumber versus grid resolution for FDTD and dispersion enhanced MOC scheme for $\nu = 3/4$.

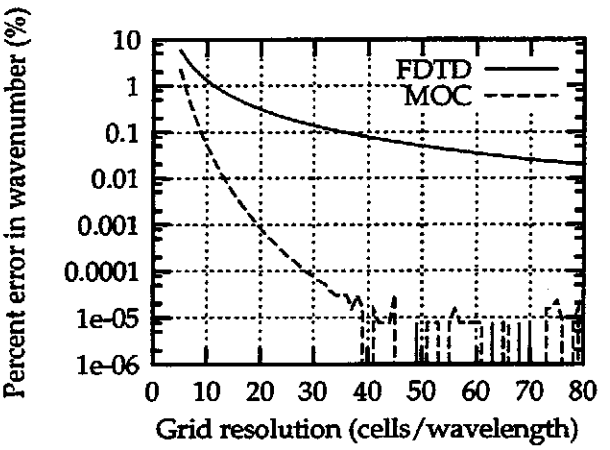

Figure 11: Same as Figure 10 except with $\nu = 1/2$.

Note the remarkable improvement in phase errors for the enhanced scheme over FDTD, even at coarse grid resolutions of 10 cells/wavelength. Although Figure 3 shows that the dispersion errors for both FDTD and the MOC schemes are relatively insignificant for reasonable grid spacings, with problems involving propagation over large distances, these

phase errors can become substantial. The improvement in phase error is generally a factor of 50 for $\nu = 3/4$, except around 25 cells/wavelength where it is a factor of 5,000 lower. The optimum range is 20-30 cells/wavelength where the dispersion error is about 500 times lower than FDTD. In Figure 11 where $\nu = 1/2$, the phase error improvement is anywhere from 500-5,000 times lower than FDTD. Similar improvements were observed at other Courant numbers in the range $0.5 \leq \nu < 1$. It is worthy to note that this low phase error scheme was developed using only a first-order ODE solver. Practical implementation of this enhanced scheme simply involves applying the parametric interpolation formula of (45) using the MOC update equations in place of $f_1(k)$ and $f_2(k)$. The dispersion enhancement depends on wavenumber, Courant number, and on the wave propagation angle for nonuniform grids and multidimensional applications. In the present work, the dispersion was optimized versus grid resolution given specific values of wavenumber and Courant number. This dispersion optimization approach can be extended to lower dispersion errors in complex multi-dimensional applications by employing an optimization procedure such as a genetic algorithm to search the parameter space. It may be sufficient to optimize dispersion properties in the multidimensional case for the highest frequency in the excitation sources versus grid resolution and wave propagation angle. Frequencies below the maximum will already be oversampled and will have lower dispersion errors, even without optimization. For a one-dimensional nonuniform grid, phase errors can be optimized in the Fourier sense for various values of ν. A Lagrange interpolation polynomial can be obtained to find the value of α given the local value of ν at each grid point. Implementation and testing of the enhanced scheme for 1D, 2D and 3D problems is currently under development.

6 Conclusions

This paper has demonstrated use of the theory of characteristics to develop numerical algorithms for solutions of Maxwell's time dependent curl equations. This class of algorithms can also easily be combined parametrically for significant reduction in phase errors over current FDTD schemes. The numerical MOC was adapted from the solution of fluid dynamics problems to the solution of Maxwell's time dependent curl equations based upon different interpolation schemes in the initial data surface. A dispersion enhanced MOC algorithm was also developed by parametric combination of the two "standard" MOC algorithms to provide phase errors 50-5,000 times lower than FDTD. This capability provides a significant advancement in the accuracy level of finite difference CEM solutions. The one-dimensional model problem results demonstrated that the numerical MOC is promising for extension and application to realistic three-dimensional problems involving PEC and lossy dielectric materials. Future extensions of this approach include treatment of frequency dependent media, nonlinear and magnetic materials and implementation on curvilinear grids. The extension of this approach to two and three-dimensional problems is currently under investigation.

References

[1] K. S. Yee, "Numerical solution of initial boundary value problems involving Maxwell's equations in isotropic media", *IEEE Trans. Antennas Propagat.*, vol. 14, no. 3, pp. 302–307, 1966.

[2] K. S. Kunz and R. J. Luebbers, *The Finite Difference Time Domain Method for Electromagnetics*, CRC Press, Boca Raton, FL, 1993.

[3] A. Taflove, *Computational Electrodynamics: The Finite-Difference Time-Domain Method*, Artech House, Boston, MA, 1995.

[4] Allen Taflove, editor, *Advances in Computational Electrodynamics: The Finite-Difference Time-Domain Method*, Artech House, New York, 1998.

[5] N. K. Madsen and R. W. Ziolkowski, "A modified finite-volume technique for Maxwell's equations", Tech. Rep. UCRL-98495, Lawrence Livermore National Laboratory, 1988.

[6] N. K. Madsen and R. W. Ziolkowski, "A three-dimensional modified finite volume technique for Maxwell's equations", *Electromagnetics*, vol. 10, no. 1/2, pp. 147–161, 1990.

[7] R. Holland, V. P. Cable, and L. C. Wilson, "Finite-volume time-domain (FVTD) techniques for EM scattering", *IEEE Trans. Electromagn. Compat.*, vol. 33, no. 4, pp. 281–294, 1991.

[8] R. Noack and D. A. Anderson, "Time domain solutions of Maxwell's equations using a finite-volume formulation", in *AIAA Meeting*, Reno, NV, Jan. 1992.

[9] C. H. Chan and J. T. Elson, "A vertex-based finite-volume time-domain method for analyzing waveguide discontinuities", *IEEE Microwave Guided Wave Lett.*, vol. 3, no. 10, pp. 372–374, 1993.

[10] D. J. Riley and C. D. Turner, "Finite-volume hybrid-grid (FVHG) technique for the solution of transient Maxwell's equations", *Applied Computational Electromagnetics Soc. Newsletter*, vol. 9, no. 2, pp. 25–32, 1994.

[11] K. S. Yee and J. S. Chen, "Conformal hybrid finite difference time domain and finite volume time domain", *IEEE Trans. Antennas Propagat.*, vol. 42, no. 10, pp. 1450–1455, 1994.

[12] K. S. Yee and J. S. Chen, "Hybrid finite difference time domain and finite volume time domain in solving Maxwell's equations", in *11th Annual Review of Progress in Applied Computational Electromagnetics*, Monterey, CA, Mar. 1995, vol. 1, pp. 453–464.

[13] D. J. Riley and C. D. Turner, "Local tetrahedron modeling of microelectronics using the finite-volume hybrid-grid tecnique", in *12th Annual Review of Progress in Applied Computational Electromagnetics*, Monterey, CA, Mar. 1996, vol. 1, pp. 536–554.

[14] M. A. Jensen and Y. Rahmat-Samii, "Finite-difference and finite-volume time-domain techniques: Comparison and hybridization", in *IEEE Antennas and Propagat. Soc. Int. Symp.*, Baltimore, MD, July 1996, vol. 1, pp. 108–111.

[15] M. A. Jensen and Y. Rahmat-Samii, "Finite difference and finite volume time domain techniques in electromagnetics: A comparitive study", *Radio Sci.*, vol. 31, no. 6, pp. 1823–1836, 1996.

[16] S. G. García, T. M. Hung-Bao, B. G. Olmedo, and R. G. Martín, "Volume-conformation method to study scattering by PEC objects with FDTD", *IEE Proc. H, Microw. Antennas Propag.*, vol. 143, no. 2, pp. 131–136, 1996.

[17] D. J. Riley and C. D. Turner, "VOLMAX: A solid-model-based, transient volumetric Maxwell solver using hybrid grids", *IEEE Antennas Propagat. Magazine*, vol. 39, no. 1, pp. 20–33, 1997.

[18] P. Bonnet, X. Ferrieres, F. Paladian, J. Grando, J. C. Alliot, and J. Fontaine, "Electromagnetic wave diffraction using a finite volume method", *Electron. Lett.*, vol. 33, no. 1, pp. 31–32, 1997.

[19] K. S. Yee and J. S. Chen, "The finite-difference time-domain (FDTD) and the finite-volume time-domain (FVTD) methods in solving Maxwell's equations", *IEEE Trans. Antennas Propagat.*, vol. 45, no. 3, pp. 354–363, 1997.

[20] M. B. Abbott, *An Introduction to the Method of Characteristics*, American Elsevier, New York, 1966.

[21] J. D. Hoffman, *Numerical Methods for Engineers and Scientists*, McGraw-Hill, New York, 1992.

[22] D. S. Butler, "The numerical solution of hyperbolic systems of partial differential equations in three independent variables", *Proc. of the Royal Soc. of London*, vol. 255A, pp. 232–252, 1960.

[23] J. D. Hoffman, "The method of characteristics applied to unsteady one-, two- and three-dimensional flows", Tech. Rep. TR-80-07, Thermal Sciences and Propulsion Center, School of Mechanical Engineering, Purdue Univ., 1980.

[24] D. L. Marcum and J. D. Hoffman, "Calculation of unsteady three-dimensional subsonic/transonic inviscid flowfields by the method of characteristics", in *AIAA 22nd Aerospace Sciences Meeting*, Reno, NV, Jan. 1984, vol. AIAA 84-0440.

[25] D. L. Marcum and J. D. Hoffman, "Calculation of viscous nozzle flows by the unsteady method of characteristics", in *AIAA 23rd Aerospace Sciences Meeting*, Reno, NV, Jan. 1985, vol. AIAA 85-0131.

[26] D. L. Marcum and J. D. Hoffman, "Calculation of three-dimensional flowfields by the unsteady method of characteristics", *AIAA Journal*, vol. 23, no. 10, pp. 1497–1505, Oct. 1985.

[27] C. P. Kentzner I. H. Parpia and M. H. Williams, "Multidimensional time dependent method of characteristics", *Computers and Fluids*, vol. 16, no. 1, pp. 105–117, 1988.

[28] V. Shankar, W. F. Hall, and A. Mohammadian, "A time-domain differential solver for electromagnetic scattering problems", *Proc. IEEE*, vol. 77, no. 5, pp. 709–721, 1989.

[29] W. F. Hall V. Shankar and A. H. Mohammadian, "A three-dimensional Maxwell's equation solver for computation of scattering from

layered media", *IEEE Trans. Magnetics*, vol. 25, no. 4, pp. 3098–3103, July 1989.

[30] W. F. Hall V. Shankar and A. H. Mohammadian, "A CFD-based finite-volume procedure for computational electromagnetics - interdisciplinary applications of CFD methods", vol. AIAA Paper 89–1987CP, 1989.

[31] W. F. Hall V. Shankar and A. H. Mohammadian, "A time-domain, finite-volume treatment for the Maxwell equations", *Electromagnetics*, vol. 10, pp. 127, 1990.

[32] W. F. Hall V. Shankar and A. H. Mohammadian, "CFD spinoff-computational electromagnetics for radar cross section (RCS) studies", vol. AIAA Paper 90–3055CP, 1990.

[33] V. Shankar, "A gigaFLOP performance algorithm for solving Maxwell's equations of electromagnetics", vol. AIAA paper 91–1578CP, 1991.

[34] J. S. Shang, "Characteristic based methods for the time-domain Maxwell equations", in *AIAA 29th Aerospace Sciences Meeting & Exhibit*, Reno, NV, Jan. 1991, vol. AIAA 91-0606.

[35] J. S. Shang, "A characteristic-based algorithm for solving 3-d time-domain Maxwell equations", in *AIAA 30th Aerospace Sciences Meeting & Exhibit*, Reno, NV, Jan. 1992, vol. AIAA 92-0452.

[36] J. S. Shang, "A fractional-step method for solving 3-d time-domain Maxwell equations", in *AIAA 31st Aerospace Sciences Meeting & Exhibit*, Reno, NV, Jan. 1993, vol. AIAA 93-0461.

[37] J. S. Shang and D. Gaitonde, "Characteristic-based, time-dependent Maxwell equations solvers on a general curvilinear frame", in *AIAA 24th Plasmadynamics & Lasers Conference*, Orlando, FL, July 1993, vol. AIAA 93-3178.

[38] K. C. Hill J. S. Shang and D. Calahan, "Performance of a characteristic-based, 3-d time-domain Maxwell equations solvers on a massively parallel computer", in *AIAA 24th Plasmadynamics & Lasers Conference*, Orlando, FL, July 1993, vol. AIAA 93-3179.

[39] J. S. Shang and R. M. Fithen, "A comparative study of numerical algorithms for computational electromagnetics", in *AIAA 25th Plasmadynamics & Lasers Conference*, Colorado Springs, CO, June 1994, vol. AIAA 94-2410.

[40] J. S. Shang and D. Gaitonde, "Characteristic-based, time-dependent Maxwell equation solvers on a general curvilinear frame", *AIAA Journal*, vol. 33, no. 3, pp. 491–498, March 1995.

[41] J. S. Shang, "A fractional-step method for solving 3d, time-domain Maxwell equations", *Journal of Comp. Phys.*, vol. 118, pp. 109–119, 1995.

[42] J. S. Shang and R. M. Fithen, "A comparative study of characteristic-based algorithms for the Maxwell equations", *Journal of Comp. Phys.*, vol. 125, pp. 378–394, 1996.

[43] D. C. Blake and J. S. Shang, "A procedure for rapid prediction of electromagnetic scattering from complex objects", in *AIAA 29th Plasmadynamics & Lasers Conference*, Albuquerque, NM, June 1998, vol. AIAA 98-2925.

[44] Z. P. Liao, H. L. Wong, B.-P. Yang, and Y.-F. Yuan, "A transmitting boundary for transient wave analysis", *Sci. Sin., Ser. A*, vol. 27, no. 10, pp. 1063–1076, 1984.

[45] J.-P. Berenger, "A perfectly matched layer for the absorption of electromagnetic waves", *J. Comput. Phys.*, vol. 114, no. 1, pp. 185–200, 1994.

[46] J. E. Fromm, "A method for reducing dispersion in convective difference schemes", *Journal of Comp. Phys.*, vol. 3, pp. 176–189, 1968.

[47] M. F. Hadi, M. Piket-May, and E. T. Thiele, "A modified FDTD (2,4) scheme for modeling electrically large structures with high phase accuracy", in *12th Annual Review of Progress in Applied Computational Electromagnetics*, Monterey, CA, Mar. 1996, vol. 2, pp. 1023–1030.

[48] M. F. Hadi and M. Piket-May, "A modified FDTD (2,4) scheme for modeling electrically large structures with high-phase accuracy", *IEEE Trans. Antennas Propagat.*, vol. 45, no. 2, pp. 254–264, 1997.

[49] S. K. Lele, "Compact finite difference schemes with spectral-like resolution", *Journal of Comp. Phys.*, vol. 103, pp. 16–42, 1992.

[50] D. Gaitonde and J. S. Shang, "High-order finite-volume schemes in wave propagation phenomena", in *AIAA 27th Plasmadynamics & Lasers Conference*, New Orleans, LA, June 1996, vol. AIAA 96-2335.